JABFM
eISSN 2280-8000

J Appl Biomater Funct Mater 2017; 15(3): e223-e235
DOI: 10.5301/jabfm.5000347

ORIGINAL RESEARCH ARTICLE

Open Access

Bone response to porous alumina implants coated with bioactive materials, observed using different characterization techniques

Claudia C. Camilo[1], Celey A.E. Silveira[2], Rafael S. Faeda[3], João M.D. de Almeida Rollo[4], Benedito de Moraes Purquerio[1], Carlos Alberto Fortulan[1]

[1] Department of Mechanical Engineering, University of São Paulo, São Carlos, SP - Brazil
[2] Rheumatology Division, FMU, University of São Paulo, São Paulo, SP - Brazil
[3] Department of Diagnosis and Surgery, School of Dentistry of Araraquara, São Paulo State University, Araraquara, SP - Brazil
[4] Interunits Postgraduate Program in Bioengineering, University of São Paulo, São Carlos, SP - Brazil

ABSTRACT

Background: Implants or implantable devices should integrate into the host tissue faster than fibrous capsule formation, in which the design of the interface is one of the biggest challenges. Generally, bioactive materials are not viable for load-bearing applications, so inert biomaterials are proposed. However, the surface must be modified through techniques such as coating with bioactive materials, roughness and sized pores. The aim of this research was to validate an approach for the evaluation of the tissue growth on implants of porous alumina coated with bioactive materials.
Methods: Porous alumina implants were coated with 45S5 Bioglass® (BG) and hydroxyapatite (HA) and implanted in rat tibiae for a period of 28 days. Ex vivo resections were performed to analyze osseointegration, along with histological analysis, Scanning Electron Microscopy with Energy Dispersive X-Ray spectroscopy (SEM-EDX) line scanning, radiography and biomechanical testing.
Results: Given that the process of implant integration needs with the bone tissue to be accelerated, it was then seen that BG acted to start the rapid integration, and HA acted to sustaining the process.
Conclusions: Inert materials coated with bioglass and HA present a potential for application as bone substitutes, preferably with pores of diameters between 100 µm and 400 µm and, restrict for smaller than 100 µm, because it prevents pores without organized tissue formation or vacant. Designed as functional gradient material, stand out for applications in bone tissue under load, where, being the porous surface responsible for the osseointegration and the inner material to bear and to transmit the loads.

Keywords: Bioactive glass, Coated surface, Hydroxyapatite, Osseointegration, Porous alumina implants

Introduction

Bone tissue engineering is a promising area in the regeneration of bone, combining stem and progenitor cells and biologically active factors (e.g., growth factors) in a scaffold to obtain bone grafts to facilitate bone regeneration (1). Biomaterial scaffolds need to integrate into the host tissue without the formation of a fibrous capsule and to present certain mechanical properties and shapes; ideally, they should mimic the natural extracellular matrix as much as possible, in terms of biochemistry, macrostructure and nanoscale and microscale surface topographies. The bone–implant interface is one of the biggest challenges in the design of implants (1-3). However, there are studies showing good bone regeneration in vivo using porous scaffolding (4, 5).

Kim et al experimented with hydroxyapatite (HA)/alumina bilayered porous scaffold and concluded that a passage-like medullary canal appeared to be important for blood circulation to improve the rate of bone regeneration (5).

According to Hench (2), the potential for a new generation of high strength, low elastic modulus, highly bioactive glass ceramics exists. However, this new class of bioactive glass ceramics must be investigated as to the effects on their strength of the environment under load conditions, before they can be designed for load-bearing applications with predictable low failure rates (6).

Numerous papers have considered that the surface modification of implants can enhance implant fixation, and several

Accepted: March 6, 2017
Published online: May 24, 2017

Corresponding author:
Dr. Carlos Alberto Fortulan
University of Sao Paulo, Department of Mechanical Engineering
400, Trabalhador Sãocarlense
São Carlos, SP, 13560-970 BR, Brazil
cfortula@sc.usp.br.com

studies report different types of techniques for the bioactivation, such as surface coating of the inert support with bioactive materials or bilayered scaffold with HA/alumina additives (5, 7-12).

Wernike et al and Klenke et al have investigated qualitatively and quantitatively angiogenesis in ceramic scaffolds due to its importance in bone formation and osseointegration (11, 12). Moreover, in a study of alumina and genetic damage, Kido et al concluded that the implantation of alumina in rat tibiae did not induce genetic damage in blood liver or kidney, highlighting the potential in vivo for application of this biomaterial as a bone substitute (13).

Alumina ceramic (Al_2O_3) is a material with high mechanical strength, high levels of stiffness and excellent corrosion resistance, which are characteristics that make the material more acceptable for biomedical applications in cases requiring inertia. However, these materials are considered near to inert and do not show osteogenic properties (14). To try to overcome these limitations, some composite materials were developed from 2 or more materials to obtain the properties of interest in a single material (15).

For the present study, aiming at the development of bone substitutes with improved mechanical properties and, at the same time, presenting high levels of bioactivity, it was hypothesized that alumina scaffolds coated with HA and 45S5 bioglass® (BG) would present good osseointegration and that, to preserve the mechanical properties, only a surface layer would be necessary for anchoring. Toward this objective, it would be necessary to determine the ideal thickness of a porous layer and so propose a concept of implants with a dense core and porous surface transition as functional gradient. The aim of this research, then, was to validate an approach for the evaluation of the tissue growth on implants of extreme hardness – namely, porous alumina coated with bioglass BG and HA, to unite osseointegration and osteoconduction in an implant and, thus, to determine an effective porous thickness with osteogenic potential.

Methods

To certify the efficiency of osseointegration using different characterization techniques, porous alumina implants were manufactured coated with HA and BG to improve osseointegration. The morphology of the pores as well as the porosity of the material became key parameters for good tissue–implant integration. The implants were implanted in rat tibiae for a period of 14 and 28 days. After resection, the following techniques were performed to analyze the osseointegration: histology, radiography, scanning electron microscopy–energy-dispersive X-ray (SEM-EDX) line scanning and biomechanical testing.

Manufacturing of implants: coated and uncoated porous alumina

The manufacture of implants used an approach similar to that reported by Camilo et al in 2009 (15) and is briefly summarized here. The method adopted has the advantage of providing implants with good mechanical properties, combined with high reproducibility, homogeneity and machinability before sintering.

To evaluate the effect of coating alumina ceramic scaffolds with bioactive materials, 2 kinds of scaffolds were prepared: coated scaffolds and uncoated scaffolds. These used 2 different ceramic slurries: alumina slurry and bioactive slurry (HA/bioglass).

For the alumina slurry we selected calcined alumina A1000-SG (Almatis Inc.) as the structural component and sucrose (LABYNTH) as the pore-forming agent. The sucrose particles were classified into 2 ranges of sieve screen sizes (177 < size A <300 μm and 300 μm < size B <600 μm). The ceramic slurry was created in a ball mill in 2 stages. First, milling for 6 hours into a polyethylene jar mill (useful volume: 100 mL, media content: 400 g of Ø6-mm zirconia balls) into which was added 30 mL of alumina, 5 mL of polyvinyl butyral (PVB; BUTVAR B98) (as binder) and 65 mL of isopropyl alcohol (as PVB solvent and liquid phase). Second, to obtain the desired 70 vol% porosity in scaffold, we added 82 vol% (82 mL) of sucrose (50% size A and 50% size B) to the slurry and mixed for an additional 5 minutes in the ball mill.

For the bioactive slurry we used HA (6.6 vol%; cat. no. 289396; Sigma-Aldrich), bioglass (3.4 vol%; 45S5 Bioglass®; Biogran), PVB 0.3 vol% and isopropyl alcohol (89.7 vol%), milled in a vibratory mill into a polyethylene jar (useful volume: 20 mL, media content: 120 g of Ø3-mm zirconia balls) for 170 hours.

Uncoated scaffolds

The alcohol of alumina slurry was evaporated using an air flow heat gun at a temperature of around 80°C, and the ceramic–sucrose agglomerates were manually granulated. The granules were pressed in an axial press using cylindrical molds at 10 MPa followed by isostatic pressing at 100 MPa. Sucrose particles were partially removed during leaching with distilled water, and the remaining particles were burned off during presintering. The uncoated scaffold samples were sintered at a temperature of 1550°C for 2 hours. The consequent increase in grain size and decrease in porosity promoted the desired porosity to reach close to 70% (45% open porous) with interconnected and angled porosity and a compressive strength of 43 ± 17 MPa (16).

Coated scaffolds

To create coated scaffolds, the pores of uncoated scaffolds were infiltrated under vacuum with the bioactive slurry (HA/BG), followed by drying in an oven at 100°C for 2 hours and firing at 900°C in a furnace for 1 hour to guarantee the coating adhesion. The result was bodies with a porosity of 65% (40% open porous) and compressive strength of 53 ± 20 MPa (16).

The final size of both the coated and uncoated scaffold implants was 2.5-mm diameter (mean 2.52 ± 0.05) and 1.5-mm height (mean 1.48 ± 0.22). Both were sterilized in an autoclave with moist heat at 121°C for 20 minutes.

Chemical and surface characterization of implants

Chemical analysis: EDX spectroscopy

In the chemical analysis, using EDX, semiquantitative determination of Ca, P, Al and Si was performed to verify the

introduction of the bioactive impregnated alumina substrate. This test was carried out on an LEO1430 scanning electron microscope (SEM) with an OXFORD detector, operating at 20 kV.

Surface roughness

Dimensional images of the surface of the coated and uncoated porous scaffold implants were obtained on a profilometer (Wyko NT 1100; Veeco). The parameters average roughness (Rm) and total roughness (Rt) were obtained. Differences between the samples were considered statistically significant according to a paired *t*-test with a p value <0.05.

Animals and implantation of biomaterials

In vivo procedures related to the animal experiments were approved by the National Commission of Research Ethics of the Clinical Hospital of Medicine School at the University of São Paulo (CAPPesq Protocol n° 0218/09).

Coated and uncoated scaffold implants were compared in the in vivo study. The site for the bone defect and implantation of the biomaterial was the tibia. The test animals fitted with implants were adult male Wistar rats (*Rattus norvegicus albinus*), body mass 260-300 g (285.39 ± 17.42), aged 8-9 weeks, in generally good condition and with normal motility. For the treatment data, 5 animals from each group were used in each experimental period, except for the control-control group (no implant), in which fewer animals were used because the defects (just the hole, without implant) was applied to both tibiae, even so, both were subject to the same ex vivo histological analysis. Water and food were provided ad libitum. The experimental periods were 2 and 4 weeks, in accordance with ISO 10993-6 for studies of short periods. The groups were named according to the implants received, as shown in Table I.

The animals were anesthetized with ketamine and xylazine (40 mg/kg and 5 mg/kg, respectively) with a 1:1 dose (20 mL/100 g) administered intraperitoneally.

A defect was created in the left tibia and another defect in the right tibia of each animal, as follows. A skin incision was made along the limb on the medial and proximal tibia, followed by a divulsion of the skin until the tibia could be seen. Defects 1 and 2 were carried out to the left tibia and right tibia, respectively. This point was drilled to obtain the defect in the unicortical tibial shaft, and the punch device shown in Figure 1 was used. The drilling was carried out with a drill perpendicular to the bone, and at the time of drilling, sterile saline was applied to the defect area. The diameter of the defect was approximately 2.5 mm.

To insert the implant in the defect volume, the implant was manually inserted applying digital pressure. After the experimental periods, the animals were euthanized in a carbon dioxide chamber. The right tibia was sent for biomechanical push-out tests to measure shear strength. The left tibia was sent for histological analysis, high-definition X-ray and analysis of chemical elements by EDX line scan.

Push-out test

A biomechanical push-out test was applied to quantify the interface-bonding shear strength between implant and bone and show the degree of osseointegration (16-18). The test was performed using an EMIC machine with a load of 500 kilogram-force (kgf [5 kN]), at a temperature of 23°C, with a 450 kgf scale and a test speed of 0.5 mm/min. Figure 2 shows a schematic of the test (Fig. 2A) and photographs of the removed tibia's contralateral cortex (Fig. 2B) and the running test (Fig. 2C). The tests ended after reaching the maximum force determined by the subsequent drop in the curve. The shear stress (τ) was calculated using Equation [1], with the following values: implant diameter (2.5 mm), punch device diameter (2.0 mm), thickness of cortical bone (mean 0.97 ± 0.1 mm) and maximum force (*F*).

TABLE I - Designation of experimental groups during in vivo studies

Group	14-day implantation period	28-day implantation period
G1 – Coated, no. of animals	7	7
G2 – Uncoated or control, no. of animals	7	7
G3 – Control-control, no. of animals	5	2

G1 = group with implant infiltrated into both tibiae (coated scaffolds); G2 = group with control implants (uncoated scaffolds); G3 = group with bone defects in both tibiae, without implantation.

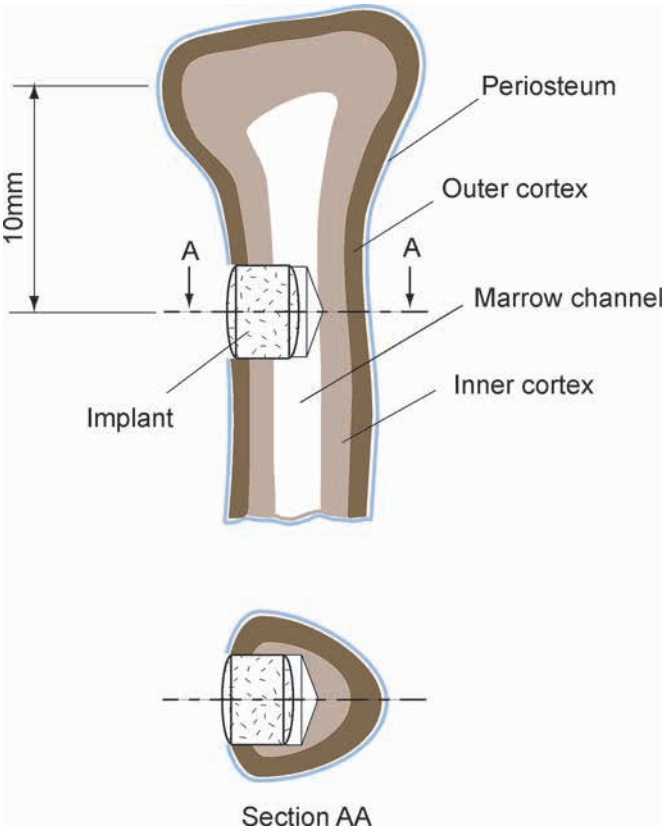

Fig. 1 - Schematic of implant insertion into the bone, showing the defect created in the cortical bone.

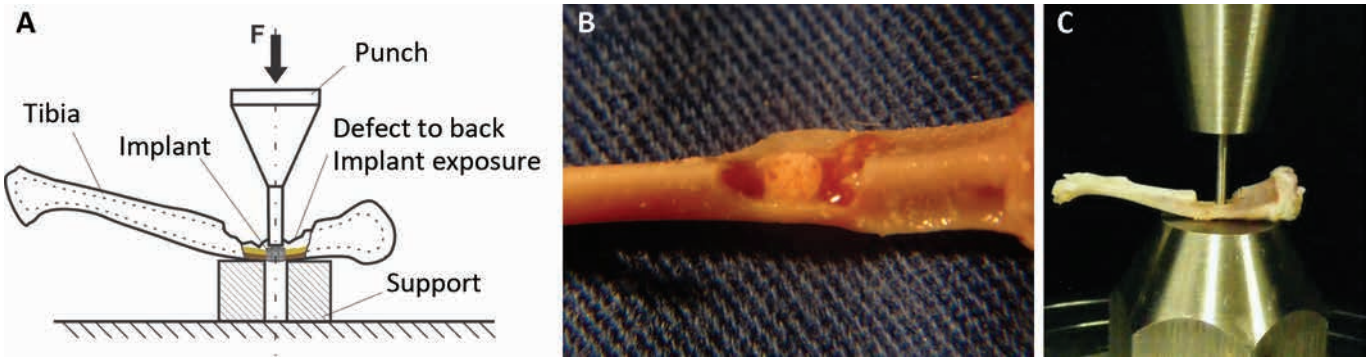

Fig. 2 - Biomechanical push out test: (**A**) schematic test; (**B**) the removed tibiae contralateral cortex; (**C**) the running test.

$$\tau = \frac{F}{S} \qquad \text{Eq. [1]}$$

where τ is the shear stress, F is the maximum strength and S is the actual implant surface area in contact with surrounding bone (S = πdh; where d is the diameter of the puncher and h is the height of the implant). The puncher diameter (smaller than the sample diameter) is considered more representative because the bone interface for effective bone integration samples is more resistant than the innermost region, where the shear in fact occurs.

Preparation of tibiae for histological analysis of mineralized tissue

Tibiae were dehydrated in a graded series of alcohol solutions from 70% to 100% and immersed in methylmethacrylate. Cross-sections of 450 µm were obtained using a diamond cutting band (thickness of 0.2 mm) followed by sanding down to thicknesses of 10 to 38 µm (EXAKT cutting and grinding systems). Specimens were stained with hematoxylin-eosin, and images were observed with a transmitted light microscope (Leitz-DM-RX; Leica). The ratio between the amount of the tissue for coated and uncoated scaffolds was determined using the software Motic 2.0.

Histology and morphometry

Morphometric analysis was performed with the software Image Tool for Windows 3.0 (UTHSCA). The observation field extended from the center of the implant to the contact surface between the bone and the implant. The perimeters of the implant surface and bone contact areas were measured as well as the perimeters of the pores and of their contact with the newly formed bone tissue. The percentage of bone contact with the implant surface was then determined according to Equation [2]:

$$\gamma_1(\%) = \frac{\alpha_1(\mu m)}{\beta_1(\mu m)}.100 \qquad \text{Eq. [2]}$$

where γ_1 is the percentage of bone contact with the implant surface, α_1 is the perimeter of the bone contact with the implant surface and β_1 is the perimeter of the implant.

Equation [3] was used to obtain the percentage of bone contact in the pores of the implants:

$$\gamma_2(\%) = \frac{\alpha_2(\mu m)}{\beta_2(\mu m)}.100 \qquad \text{Eq. [3]}$$

where γ_2 is the percentage of bone contact in the pores, α_2 is the perimeter of bone contact with the pores and β_2 is the perimeter of the pores.

The coated and uncoated implants were compared in terms of their values for their pore diameter and the perimeter of newly formed tissue in the pores.

Radiographic study

Radiographic equipment was used with the same parameters for all samples: collimation 7, time 2 minutes and focus 60. In this analysis, it was considered that the mineralized region was radiopaque and that radiotranslucence indicated low mineralization at the interface.

The radiographs were analyzed for grayscale levels at the bone–implant interface using the software Image Tool for Windows 3.0 (UTHSCA). All images were saved with the file extension .TIF, uncompressed format at 400 dpi resolution and 8-bit gray scale, which provides values between 0 and 256, where 0 is black and 256 is white with intermediate gray tones. It was considered that higher pixel numbers were equivalent to higher radiopacity, which meant greater mineralization of that particular region of the bone–implant interface analyzed.

EDX line scan

Analysis of the mineral contents was performed using Link Analytical EDX equipment (model QX 2000) coupled with a Zeiss SEM (model LEO 440). The analysis was performed with carbon coating, and a backscattered electron detector was used. A virtual line was drawn on the bone–implant interface, as well as 3 virtual lines in the porous region of the implant, to observe the distribution of the elements – i.e. phosphorus (P) and calcium (Ca) – representing bone tissue at the interface and in the implant pores. The elements verified were Ca, P, Al and Si, which indicated the presence of bone in the pores (and the absence of Al).

Results

Chemical and surface characterization

Chemical analysis: EDX

Al is present in the alumina (Al_2O_3) matrix and not in the implant coating, but oxygen is common to both components. The chemical elements present only in the implant coating were Ca, P, Si and Na – that is, elements making up the molecular structure of HA ($Ca_{10}(PO_4)_6(OH)_2$) and BG (SiO_2-CaO-P_2O_5-Na_2O). The mass proportions of the chemical elements in the alumina matrix coated with HA and BG (coated implant) can be seen in Table II.

The presence of the chemical elements common to the bioactive materials was detected and most pronounced in the middle region and on the outer edge. This is an indication of selective permeation into the sample, with higher concentrations of bioactive material on the more external surfaces. This observation is in addition to Camilo et al (16) findings, that after coated of scaffolds, they won 5 mass % by filling of the pores and increase of mechanical resistance.

Surface roughness

The arithmetic average of the absolute values for the roughness (Ra) and total roughness (Rt) as well the average and standard deviation were obtained, as shown in Table III. The implants coated with bioactive materials showed higher average roughness values compared with the uncoated implants, with the difference being more significant when compared with the total roughness.

Push-out test

The shear stress values were analyzed for differences between groups, applying the Tukey test. A p value <0.05 was considered a significant difference. The right tibia was used for the shear test.

TABLE II - Percentage distribution of chemical elements in the coated scaffolds

Chemical element	Implant region, %		
	Central	Intermediate	Most external
C	51.94	47.42	42.32
O	42.73	44.30	42.68
Al	5.07	7.88	14.54
Si	0.19	0.31	0.19*
P	0.04*	0.03*	0.12*
Ca	0.04*	0.07*	0.16
Na	ND	ND	ND
Total	100	100	100

ND = not detected.
*Sigma <2: value not significant.

TABLE III - Superficial roughness values

Roughness (µm)	Coated	Uncoated	p value*
Ra	86.20 ± 5.15	60.43 ± 5.00	0.0049
Rt	454.64 ± 54.32	481.25 ± 2.02	0.2395

Values are average and standard deviation, or p values.
Ra = roughness (arithmetic average); Rt = total roughness.
*Paired t-test, with p<0.05 considered significant.

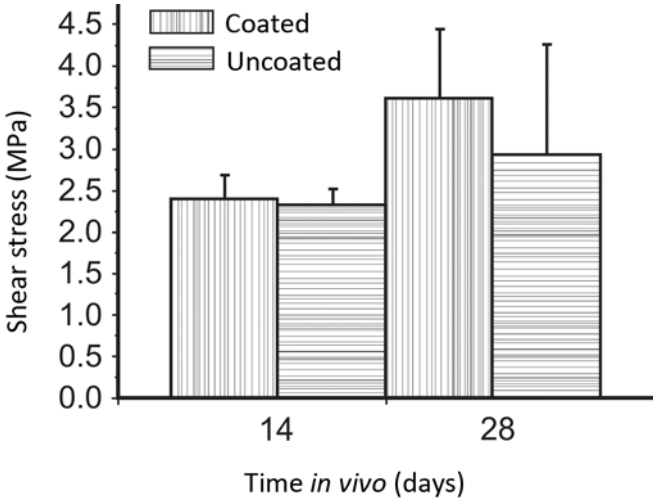

Fig. 3 - Graph of shear stress (push-out) of the implants after the trial periods of 14 and 28 days. Data expressed as mean and standard deviation.
* Significance level *p* <0.005 (Tukey test).

In the tests, the region of the implant in contact with the bone remained intact without becoming detached – that is, the implant was pushed internally and the interface did not follow it. Thus, in Equation [1], the diameter of the actuator was applied but instead of the height of the implant (h), the thickness of the cortical bone was used, since this was considered the functional surface. The results (means and standard deviation) are shown at Figure 3 and indicate that the higher the deployment time, the greater the shear stress.

As shown in Figure 3, a significant difference between 14 and 28 days was observed for the coated implant. After a period of 28 days, the value for the coated implant was 24% higher than that for the uncoated implant.

On comparing the groups with and without coating, after 14 days, there was no significant difference (p = 0.8298), and after 28 days, the value for the coating group was higher but the difference was not significant (p = 0.3244). On comparing the group with coating at different times (14 and 28 days), a significant difference was found (p = 0.0260). For the uncoated group at different times (14 and 28 days), the difference was not significant (p = 0.391).

Histology

Figure 4 shows the histological images of the porous alumina implant coated with BG and HA (Al_2O_3i) in Figure 4A,

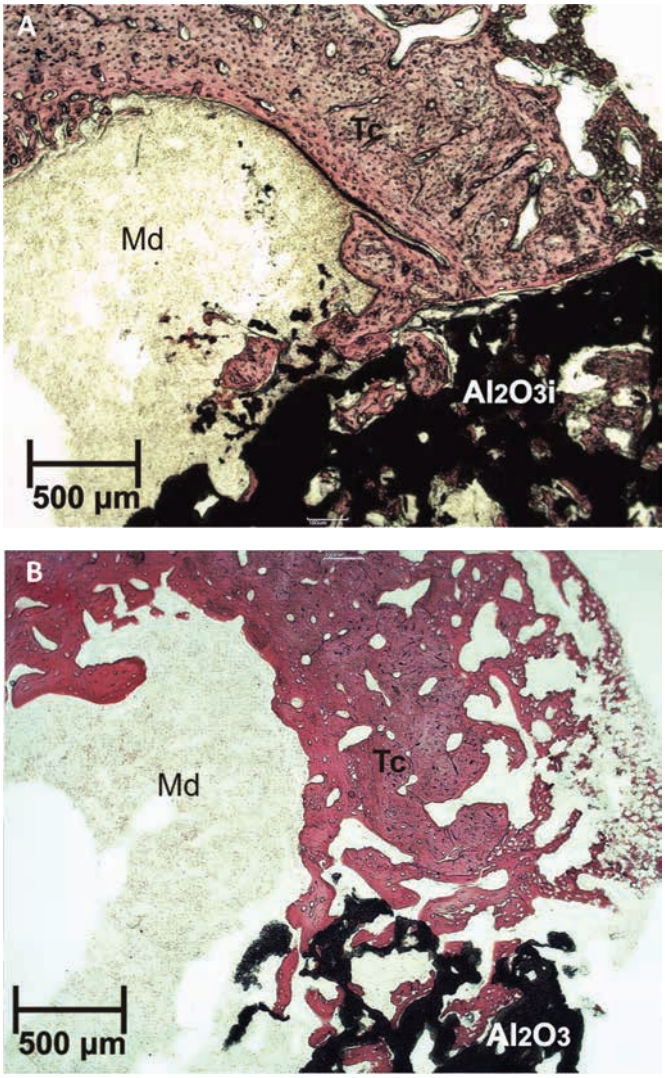

Fig. 4 - Histology images of the porous alumina implant after 14 days of implantation: (**A**) coated implant (Al_2O_{3i}); (**B**) uncoated implant (Al_2O_3). Md = bone marrow; Tc = bone.

referred to as the coated implant, and the uncoated porous alumina (Al_2O_3) in Figure 4B, after the experimental period of 14 days in the rat tibiae. Both images in Figure 4 show the bone–implant interface and the pores. In these images, bone marrow (Md) and bone (Tc) are presented at the bone–implant interface and in the pores of the implant. After 14 days, newly formed cortical bone is observed in the pore surface of both implants, but in the case of the coated implant (Fig. 4A), the tissue appears to have a greater degree of organization.

Figure 5 shows histological images of the coated implant (Fig. 5A, C) and uncoated implant (Fig. 5B, D) after the experimental period of 28 days. All images show the bone–implant interface and the pores. Bone (Tc) is present at the bone–implant interface and in the pores of the implant. Direct contact between the bone and implant can be noted in images Figure 5A and C (coated implant). However, it can be observed that in images Figure 5B and D, for uncoated implant, some pores of the bone tissue are not in direct contact with the pore walls, showing the effect of the lack of bioactive coating.

As shown in Figure 5, after 28 days, bone tissue can be observed on the surface and in the pores of both implants, but for the coated implant (Fig. 5A) and (Fig. 5C), direct contact between bone and implant can be noted, while for the control, in some pores, direct contact does not occur. There is newly formed tissue in the pores of both samples.

Morphometry

Figure 6 shows the percentages of bone contact perimeter at the implant surface. The bone contact perimeters, after 14 days of implantation, were superior in the coated compared with the uncoated implants, although the difference was not significant ($p = 0.30$). However, after 28 days, for the coated implants, the difference was significant ($p = 0.0173$). Observing the same groups, for implantation periods of 14 and 28 days, the bone contact perimeter for the coated implants increased at greater implantation times, and the difference was significant ($p = 0.0462$). For the uncoated implant, there was also an increase; however, the difference was not significant ($p = 0.4814$).

There was an increase in the percentages of bone contact in the pores of the implants for the longer period. Significant differences between the coated and uncoated groups for the periods of 14 days and 28 days could be observed ($p = 0.0402$ and $p<0.0001$, respectively).

Table IV presents the values, expressed as means and standard deviation, for the percentages of bone contact at the surface and inside the pores of the coated and uncoated implants after the 2 experimental periods. There was increased bone contact after the longer experimental period for both samples, and the difference was significant for both groups (coated group: $p<0.0001$; and uncoated group: $p = 0.0272$).

The mean pore diameter without mineralized tissue was measured after the experimental periods (Fig. 7). The values for the pore diameter were obtained to examine the influence of pore size on the tissue-formation process during the experimental periods studied. The mean diameters of 10 pores without organized tissue or with granulation tissue ("vacant") were measured for each sample. Three measurements were obtained for each vacant pore diameter.

A total of 40 pores were analyzed to obtain the mean diameter of the vacant pores (pores without organized tissue or with granulation tissue). The results showed that 28 pores had diameters smaller than 100 µm, 8 between 100 µm and 200 µm, 2 between 200 µm and 300 µm and 2 between 300 µm and 400 µm. In the case of the coated implants, all pores without organized tissue had mean pore diameters of less than 150 µm for both periods. For the uncoated implants, the pores were smaller than 357 µm in diameter after 28 days, and all pores of less than 162-µm diameter had no organized tissue.

The HA and BG coating was observed in the pores of the alumina with 70% porosity (coated implants), which allowed the growth of newly formed bone tissue after 14 days in pores larger than 100 µm. However, for the control or uncoated implants, bone tissue was observed in the pores with

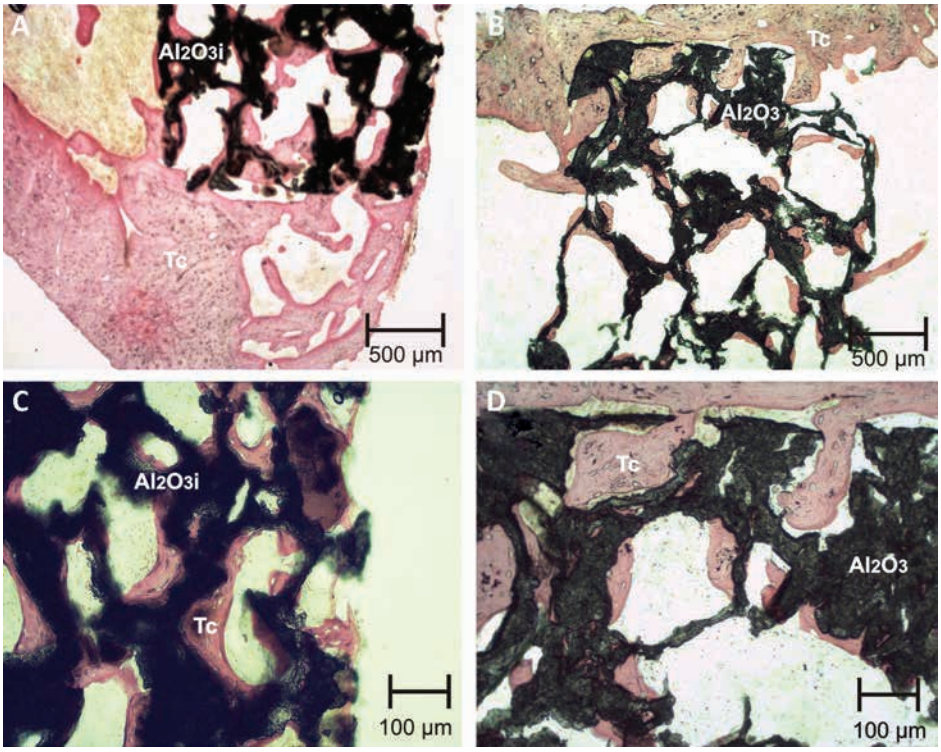

Fig. 5 - Histological images of implants of porous alumina coated with bioglass and hydroxyapatite (Al_2O_{3i}) (**A**, **C**) and of porous alumina (control or uncoated implant – Al_2O_3) (**B**, **D**), after the experimental period of 28 days in rat tibiae. The implant can be seen in black, and bone (Tc) in shades of pink. Magnification is higher in (**C, D**); hematoxylin-eosin staining.

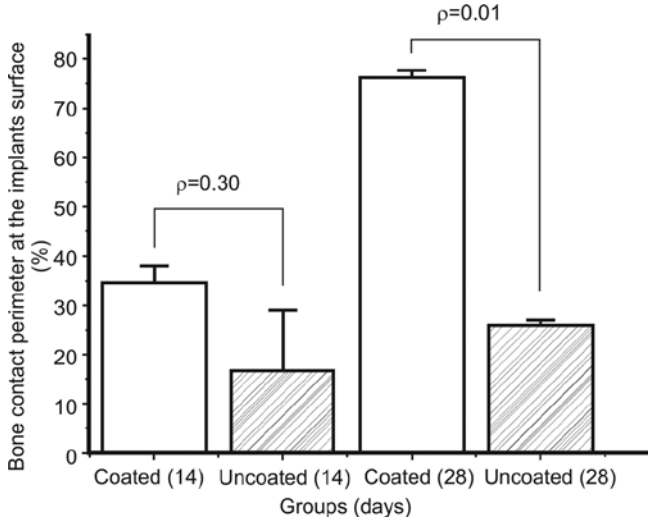

Fig. 6 - Percentages of bone contact at the surface of the implant of porous alumina coated with hydroxyapatite and bioglass and the control implant (porous alumina) after being implanted in the rat tibia. Experimental periods = 14 and 28 days. Significance level $p<0.05$.

diameters of less than 162 µm after the trial period of 28 days in the rat tibiae.

Radiographic study

Figure 8 shows a graphical interface of the sample under analysis, in this case after an implantation period of 14 days. The blue dashed circle in the X-ray is drawn over the bone–implant region, and the software counts and displays the data and histogram. Radiopacity values are presented in Table V. The values for the radiopacity at the bone–implant interface were higher for the coated implant, while the mean values revealed a larger radiopaque region. However, the maximum radiopacity values for the coated implants were higher after the 28-day period.

After 14 days, on comparing the coated and uncoated groups, the values for radiopacity were considered to indicate a significant amount of infiltration in the implant ($p<0.005$). After 28 days, higher values were obtained for the coating group, but the difference in comparison with the uncoated groups was not significant ($p = 0.0505$). The mean and standard deviation for the radiopacity values for the uncoated and coated implants are shown in Figure 9.

TABLE IV - Percentage bone contact (surface and pores) of the coated and uncoated implants after the different experimental periods

	% Bone contact at the implant surface		% Bone contact in the implant pores	
Implantation period, days	**14**	**28**	**14**	**28**
Coated	33.94 ± 4.03	76.13 ± 1.57	29.24 ± 11.18	74.54 ± 18.83
Uncoated	16.51 ± 12.39	25.84 ± 1.12	19.03 ± 12.71	31.10 ± 13.38

Values are means and standard deviation.

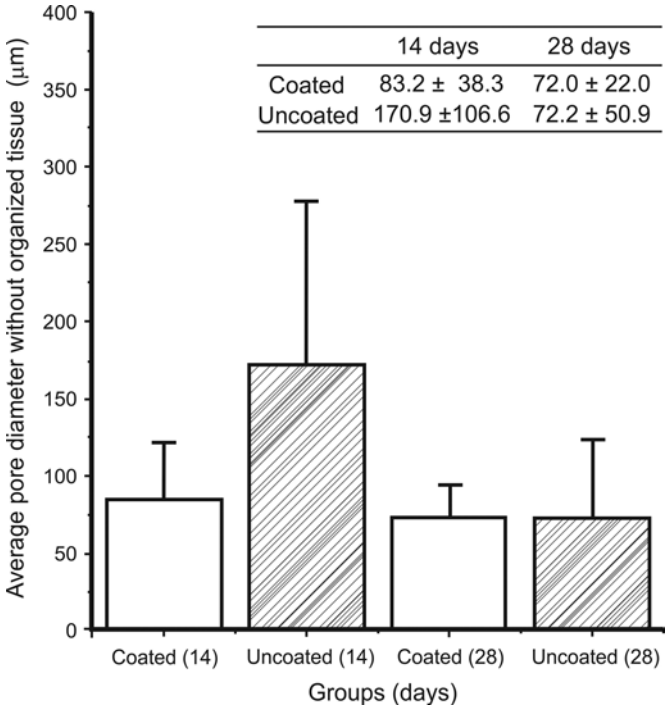

Fig. 7 - Mean diameter of pores without organized tissue or with granulation tissue ("vacant"). Of the pores analyzed with an mean diameter of less than 100 µm, 70% showed no newly formed bone tissue.

The radiographic analysis of the tibiae with implants showed a continuous interface between the implant and the bone, with greater radiopacity (greater mineralization) after the trial period of 28 days for both samples.

EDX line scan

Figure 10 shows a SEM image with details of the polished porous surface for coated implant after 28 days. Image details show a higher magnification where it is possible to observe the presence of newly formed bone tissue in the pores.

Table VI presents EDX analysis of cut and polished implants surface for all groups implanted. It can be observed from the values that the percentages of calcium and phosphorus, elements of HA, were highest for the coated implant after 28 days, which proves superior bone formation. In contrast, uncoated implant presented the highest aluminum contents (28 days) and lower relative bone formation.

A line was drawn diagonally on the image in Figure 11 from the implant pores near the bone marrow to the surface of the biomaterial implant. This is covered with calcified tissue with the morphological characteristics of cortical bone tissue.

In Figures 12 and 13, the coated implant is shown in panels A, B and C and the uncoated implant in panels D, E and F. Figure 12 shows the region of deployment for the experimental period of 14 days, and Figure 13 for the period of 28 days. Images in panels A and D show the tibia section to illustrate the positioning of the implants, and in panels B and E, the magnification is even higher. Panels C and F in each image

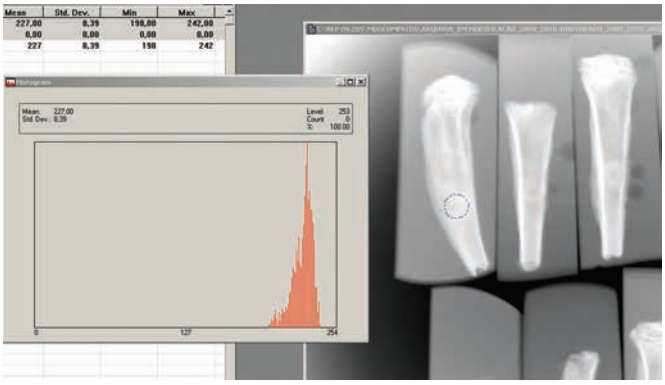

Fig. 8 - Graphical software Image Tool for Windows 3.0 (UTHSCA) used for the analysis of gray scales on X-rays for the samples after 14 days.

TABLE V - Radiopacity values from radiographic images of tibiae after trial period: coated vs. uncoated groups

Groups (n = 5)	Radiopacity (pixels)		
	Average	Minimum	Maximum
Coated, 14 days	225.8 ± 5.54	206.2 ± 10.32	240.8 ± 0.83
Uncoated, 14 days	170.4 ± 5.41	131.0 ± 13.43	218.6 ± 18.03
Coated, 28 days	220.2 ± 21.68	192.4 ± 19.67	244.4 ± 18.29
Uncoated, 28 days	188.2 ± 19.76	154.6 ± 16.27	218.4 ± 21.73

Values are in pixels (average, minimum, maximum).

show a higher magnification of the region of the implant. In Figure 12A, B, D and E, it can be noted that the implants are not covered with bone tissue after the experimental period of 14 days. In Figure 13C and F, it can be observed that the implants are covered with bone tissue.

Figure 14 shows the EDX images obtained from Figure 13C and 13F that is, of the coated and uncoated implants after 28 days of deployment. It can be observed that the bone formation in the pores of the coated implant was more concentric than is seen in the uncoated implant. The distribution of Ca and P in the samples is shown at figure 14 to the sequence of section images (coated and uncoated) and indicates that these chemical elements are both present in the pores of the HA implants. However, for the coated implants, Ca and P were distributed concentrically and in contact with the pores of the implants. In the coated implants, mineralized bone was formed in direct contact with the pore walls or the implant surface. The results of the EDX line scan suggest that, in the uncoated implants, mineralized bone tissue was present at the interface and in the pores of the implant, and there was also the presence of granulation tissue (seen in the histology examination) between the mineralized tissue and biomaterial.

Discussion

The use of a porous alumina matrix for bone implants has been previously investigated by Kim et al (19) and Naga

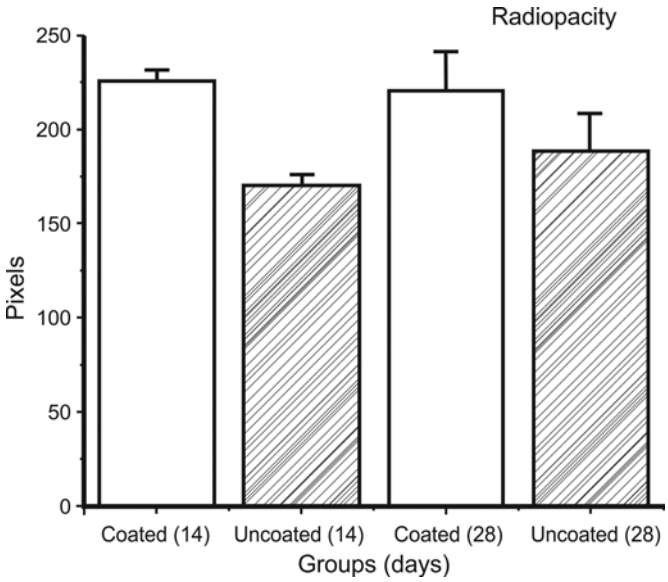

Fig. 9 - Radiopacity values (pixels): comparison between the control (uncoated porous alumina) and coated porous alumina implants, after periods of 14 and 28 days.

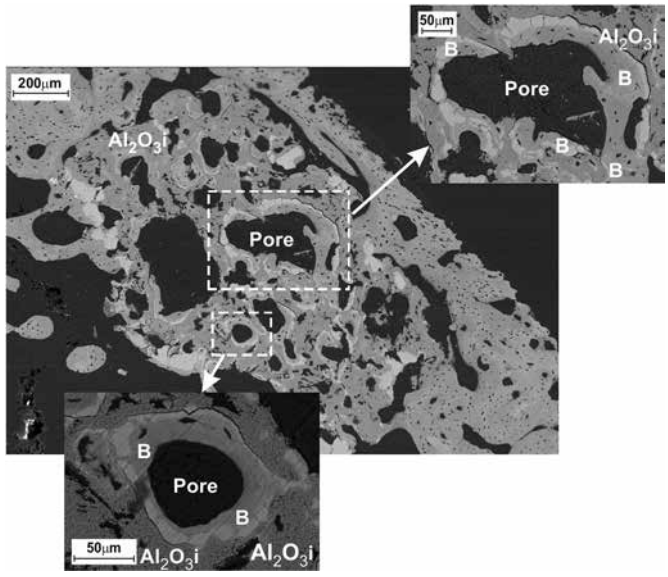

Fig. 10 - Scanning electron microscopy after coated implant trial period of 28 days. The bone tissue appears to be in direct contact with the pore walls. Regions of the implant are coated implant (Al_2O_{3i}) and bone tissue (B).

et al (10). They investigated porous alumina coated with tricalcium phosphate (TCP) and used the polyurethane (PU) foam method described in the literature for the manufacture of alumina scaffold. In this method, the foam does not offer sufficient mechanical strength for bone reconstruction. In the study reported herein, the alumina matrices were manufactured using isostatic pressing, slip casting and sintering, which provide components with greater mechanical resistance compared those created with the foam method. According to Kim et al, the use of implants made up of porous alumina coating

TABLE VI - Energy-dispersive X-ray (EDX) analysis of elements in cut and polished implants with surfaces coated and uncoated (control) after 2 experimental periods

EDX chemical element (%)	Coated		Uncoated	
	14 days	28 days	14 days	28 days
Ca	14.79	18.65	14.52	12.94
P	7.95	9.98	8.05	7.00
Si	0.98	-0.12*	-0.08*	0.04*
Al	21.90	16.51	18.92	28.87
O	54.38	54.98	58.58	51.15
Total	100	100	100	100

*Sigma <2: value not significant.

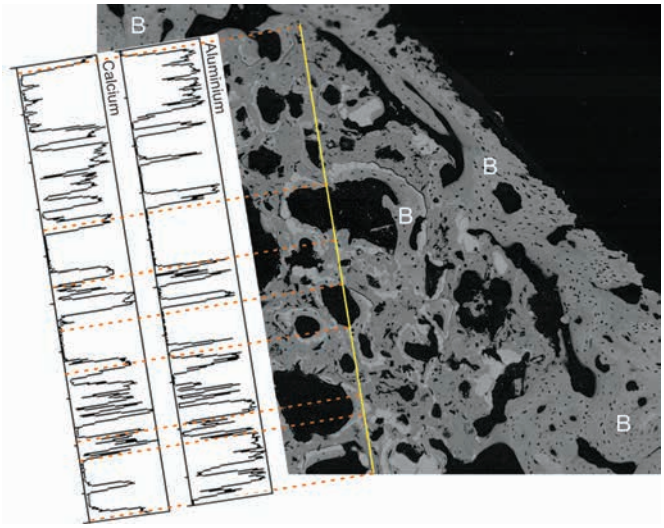

Fig. 11 - Scanning electron micrograph and energy-dispersive X-ray (EDX) line scan of coated implant after the trial period of 28 days: diagonal line across the implant. Calcium from the pores of the medullar region is present close to the surface of the implant. B = bone tissue; BM = bone marrow region.

with bioactive material promotes fixation of the implant to the host tissue (19).

The surface roughness was significantly higher for the alumina implants coated with bioactive materials, which is a favorable result. According to Kangasniemi et al, the interfacial shear strength is related to the friction between the bone and implant, which is dependent on the roughness and the contact area at the surface (20). Kam et al conducted a comparative study on the surface roughness (Ra) of implants and showed that the ceramic material presented adequate osseointegration for dental implants (21).

During the mechanical tests to determine the interfacial shear in this study, some implants fractured into 3 parts, especially after the trial period of 28 days. This phenomenon shows that the mechanical performance at the osseointegration interface and below the implant surface (0.5 mm) was

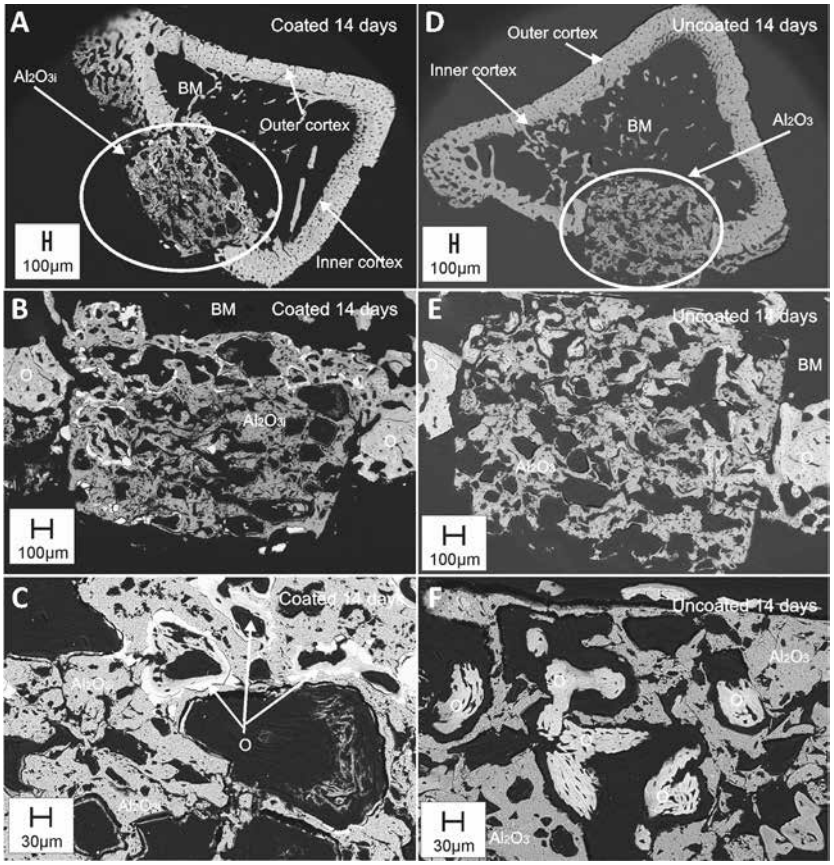

Fig. 12 - Scanning electron microscopy of tibiae with coated (**A**-**C**) and uncoated (**D**-**F**) implants, after 14-day trial period. BM = bone marrow region, B = bone tissue.

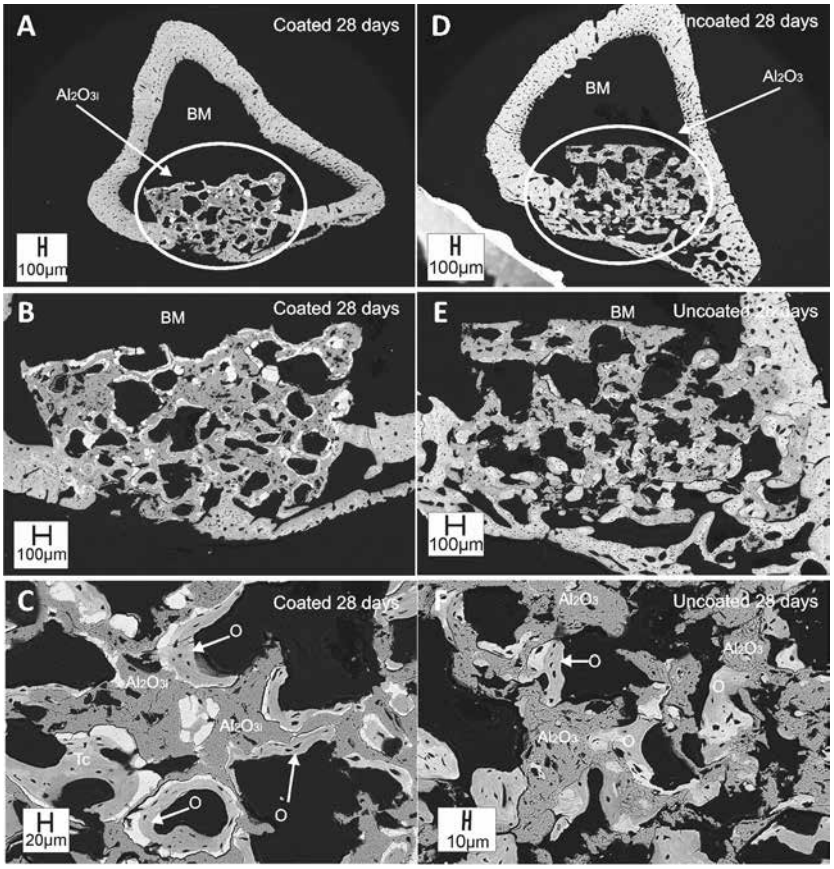

Fig. 13 - Scanning electron microscopy of tibiae with coated (**A**-**C**) and uncoated (**D**-**F**) implants, after 28-day trial period. (**A**, **D**) Section images of the tibia to illustrate the positioning of the implants. (**B**, **E**) It can be observed that the implants are covered with bone tissues. (**C**, **F**) The region of the implant where it can be observed that bone formation in the pores of the coated implant (**C**) occurred more concentrically compared with the uncoated implant (**F**).

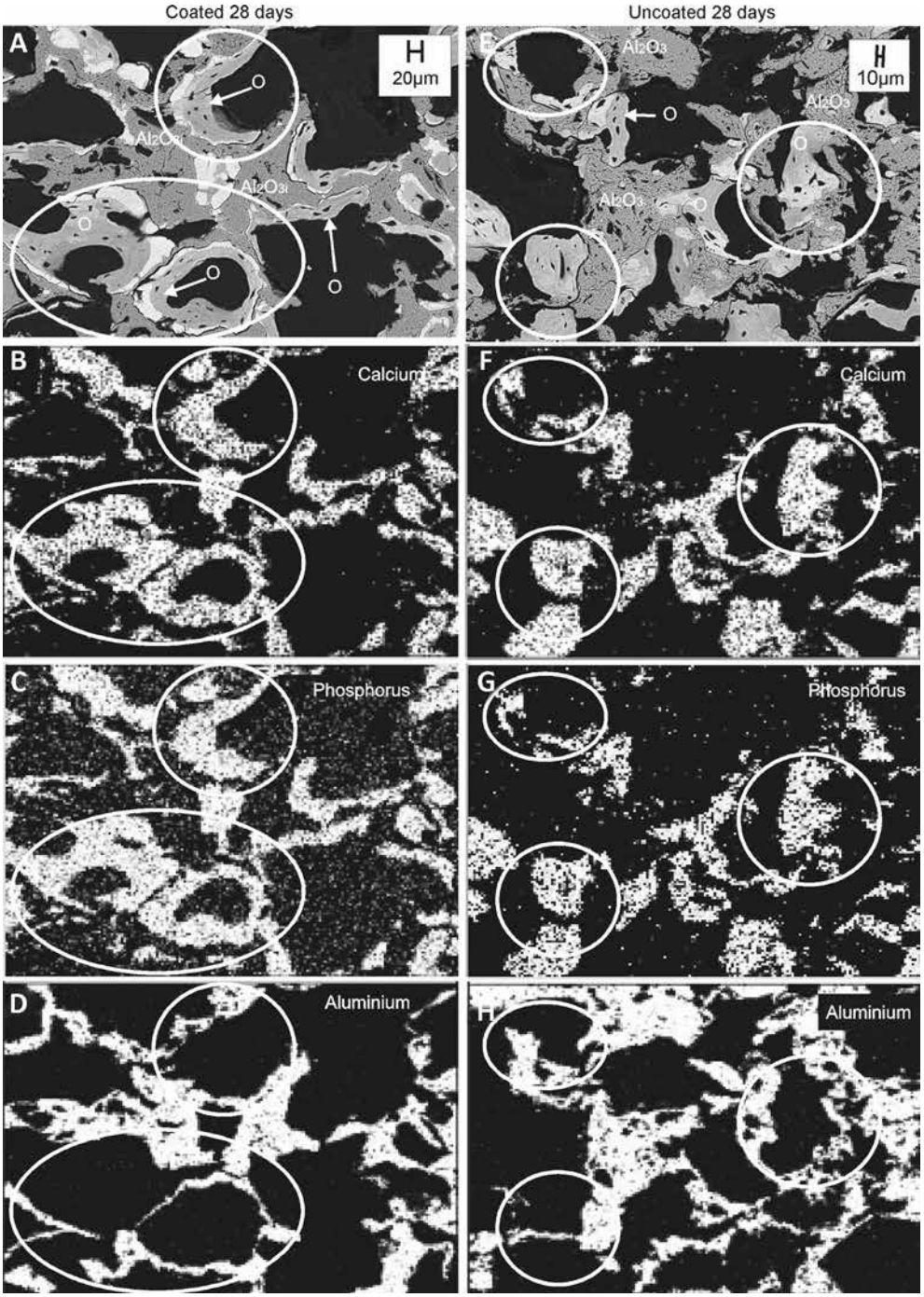

Fig. 14 - Scanning electron micrographs (**A**, **E**) , followed by energy-dispersive X-ray (EDX) images (**B**-**D** and **F**-**H**) of the coated (**A**-**D**) and uncoated (**E**-**H**) implants, after 28 days of deployment. The distribution (circles) of the chemical elements calcium (Ca), phosphorus (P) and aluminum (Al) in the sample was determined by EDX.

superior to the mechanical strength of the implant itself. These results corroborate the results of Hing et al, who found that in some cases, experimental implants may fracture into 3 or more parts after this test (22).

The interaction between bone tissue and porous or dense implants has been investigated by Anderson and by Griss et al, and interestingly, these authors reported different considerations regarding the tissue response to biomaterials (23, 24). Anderson posited that the final response of a non-porous implant is fibrosis or fibrous encapsulation and found that this was not the case for porous materials (25).

Several authors, including Jun et al, He et al, Su et al and Diefenbeck et al, have demonstrated that the osseointegration of implants can be enhanced with bioactive surfaces (4, 7-9). In the present study, the implants coated with a bioactive surface also showed a higher capacity for osseointegration.

Also, in this present study, uncoated porous alumina implants (control) were compared with those coated with bioactive materials implanted in rat tibiae. The histological, morphometric and EDX results indicated that the bone came in direct contact with the surface and the pore walls of the coated porous implants. In the case of the uncoated implants,

histology also identified the presence of tissue in the pores; however, it did not appear to be in direct continuous contact with the pore walls, as there was the presence of granulation tissue between the tissue and the implant and at some points of contact. High-definition radiography showed a radiotranslucent region at the bone–implant interface in the case of the control implants, which is indicative of lower mineralization in this region and confirms the histological results, with the presence of granulation tissue between the control implant and newly formed tissue. The grayscale radiopacity study showed greater infiltration at the interface of the implant, which indicated a higher degree of mineralization.

In a physiological environment, alumina – a material commonly used for implants – is a matrix of inert material, nonabsorbable and of extreme hardness. The porous implants with 70% porosity and coated with bioactive materials have a mechanical response to compression of 43.27 MPa (16). It was reported by Heimke that dense alumina resists up to 4,000 MPa (14).

In the histological findings of this present research, direct contact between newly formed bone tissue at the bone–implant interface and the pores of the coated implant with neovascularization was identified, with the most significant evidence being obtained for the experimental period of 28 days in rat tibiae. However, for Wernike et al, the release of vascular endothelial growth factor (VEGF) appeared to be an important factor in the promotion of biomaterial vascularization and bone formation (11). Clarkin et al noted that angiogenic growth factors did not directly stimulate osteoblast function, but instead VEGF promoted the activity of osteoblasts via the stimulation of endothelial cells (25).

In the case of the coated implants, after periods of 14 and 28 days, it was identified that newly formed bone tissue was in direct contact with the implant both at the interface and inside the pores. In the qualitative and quantitative analysis, it was observed that there was occupation of the opened pores by newly formed bone tissue. The bone–implant contact was more pronounced in samples after 28 days of deployment of the implants.

In summary, the EDX line scan results indicated that the coated implants underwent faster osseointegration than the control implants. The surface roughness of the porous alumina coated with HA/BG was compared with that of the uncoated porous alumina, and the former was significantly higher, which gives evidence for the osseointegration properties of porous alumina coated with BG and HA.

Conclusion

Porous alumina implants coated with BG and HA showed higher biocompatibility and osseointegration response than the pure alumina scaffolds.

From the ex vivo validation of the osseointegration of the coated implants, along with the histological analysis, SEM-EDX line scan, radiography and biomechanical testing, it can be concluded that considerable osseointegration occurs within 28 days of deployment in rat tibiae.

These results demonstrate that when planning the porous region of this type of functional gradient material, the pore size is of great relevance. Thus, implant designers should preferably consider pores with diameters of between 100 µm and 400 µm and restrict the formation of pores smaller than 100 µm, once, in the pores smaller than 100 µm were not observed significant organized tissue and, classically in ceramics, porosity contributes strongly to the reduction of the mechanical properties.

All techniques applied to analysis of osseointegration show that the osseointegration process was accelerated, validating the approach applied for biomaterial coating of porous alumina implants, where the coated implant presented the potential for application as bone or dental implants. This design aspect must be considered for applications in bone tissue.

Acknowledgements

The authors are also grateful to INCT-Biofabris (573661/2008-1); Dr. Silvio Eduardo Duailibi of the Department of Science and Technology, University Federal of São Paulo, São José dos Campos, SP, Brazil; and Ibero American Biomanufacturing for their support. The authors also acknowledge Dr. Suzana Beatriz V. de Mello of the School of Medicine at the University of São Paulo for assistance with the in vivo procedures.

Disclosures

Financial support: The authors gratefully acknowledge the financial support of Coordenação de Aperfeiçoamento de Pessoal de Nível Superior/Brazil (CAPES) (Contract No. PE 0652008 481500/2007-3) and Fundação de Amparo à Pesquisa do Estado de São Paulo/Brazil (FAPESP) (Process 2010/51698-0).
Conflict of interest: None of the authors has any financial interest related to this study to disclose.

References

1. Kesireddy V, Kasper FK. Approaches for building bioactive elements into synthetic scaffolds for bone tissue engineering. J Mater Chem B Mater Biol Med. 2016;4(42):6773-6786.
2. Hench LL. Bioceramics. J Am Ceram Soc. 1998;81(7):1705-1728.
3. Wu SL, Liu XM, Yeung KW, Liu CS, Yang XJ. Biomimetic porous scaffolds for bone tissue engineering. Mater Sci Eng Rep. 2014; 80:1-36.
4. Jun SH, Lee EJ, Jang TS, Kim HE, Jang JH, Koh YH. Bone morphogenic protein-2 (BMP-2) loaded hybrid coating on porous hydroxyapatite scaffolds for bone tissue engineering. J Mater Sci Mater Med. 2013;24(3):773-782.
5. Kim JM, Son JS, Kang SS, Kim G, Choi SH. Bone regeneration of hydroxyapatite/alumina bilayered scaffold with 3 mm passage-like medullary canal in canine tibia model. Biomed Res Int. 2015;2015:235108.
6. Hench LL. The future of bioactive ceramics. J Mater Sci Mater Med. 2015;26(2):86.
7. He X, Zhang YZ, Mansell JP, Su B. Zirconia toughened alumina ceramic foams for potential bone graft applications: fabrication, bioactivation, and cellular responses. J Mater Sci Mater Med. 2008;19(7):2743-2749.
8. Su B, He X, Dhara S, Mansell JP. Porous and bioactive alumina ceramics for bone grafts and tissue engineering scaffolds. Key Engineering Materials. 2007;330-332:975-978.
9. Diefenbeck M, Mückley T, Schrader C, et al. The effect of plasma chemical oxidation of titanium alloy on bone-implant contact in rats. Biomaterials. 2011;32(32):8041-8047.

10. Naga SM, Awaad M, El-Maghraby HF, El-Kady AM. Biological performance of calcium pyrophosphate-coated porous alumina scaffolds. International Journal of Applied Ceramic Technology. 2014;11(1):1-11.
11. Wernike E, Montjovent MO, Liu Y, et al. VEGF incorporated into calcium phosphate ceramics promotes vascularisation and bone formation in vivo. Eur Cell Mater. 2010;19:30-40.
12. Klenke FM, Liu Y, Yuan H, Hunziker EB, Siebenrock KA, Hofstetter W. Impact of pore size on the vascularization and osseointegration of ceramic bone substitutes in vivo. J Biomed Mater Res A. 2008;85(3):777-786.
13. Kido HW, Ribeiro DA, de Oliveira P, et al. Biocompatibility of a porous alumina ceramic scaffold coated with hydroxyapatite and bioglass. J Biomed Mater Res A. 2014;102(7): 2072-2078.
14. Heimke G. Ceramics for osseo-integrated implants. Advanced Ceramic Materials (Westerville). 1987;2(4):764-770.
15. Camilo CC, Fortulan CA, Ikegami RA, Santos AR Jr, De Purquerio BM. Manufacturing of porous alumina scaffolds with bio-glass and HAp coating: mechanical and in vitro evaluation. Key Engineering Materials. 2009;679-682.
16. Camilo CC, Fortulan CA, Parizotto NA, Purquerio BD. Porous alumina scaffolds with bioactive coating: Implants in the rat tibia and in vitro studies. Key Engineering Materials. 2009; 699-702.
17. Ogiso M, Yamamura M, Kuo PT, Borgese D, Matsumoto T. Comparative push-out test of dense HA implants and HA-coated implants: findings in a canine study. J Biomed Mater Res. 1998;39(3):364-372.
18. Takahashi K, Shiraishi N, Ishiko-Uzuka R, et al. Biomechanical evaluation of Ti-Nb-Sn alloy implants with a low Youngs modulus. Int J Mol Sci. 2015;16(3):5779-5788.
19. Kim YH, Anirban JM, Song HY, Seo HS, Lee BT. In vitro and in vivo evaluations of 3D porous TCP-coated and non-coated alumina scaffolds. J Biomater Appl. 2011;25(6):539-558.
20. Kangasniemi IM, Verheyen CC, van der Velde EA, de Groot K. In vivo tensile testing of fluorapatite and hydroxylapatite plasma-sprayed coatings. J Biomed Mater Res. 1994;28(5):563-572.
21. Kam MH, Han JS, Yang JH, Lee JB, Kim DJ, Lee WJ. Histomorphometric analysis of zirconia/alumina composite and CP titanium treaded implants in rabbit tibia. Bioceramics. 2006;18(Pts 1 and 2):309-311 and 437-440.
22. Hing KA, Best SM, Tanner KE, Bonfield W, Revell PA. Mediation of bone ingrowth in porous hydroxyapatite bone graft substitutes. J Biomed Mater Res A. 2004;68(1):187-200.
23. Anderson JM. Biological responses to materials. Annu Rev Mater Res. 2001;31(1):81-110.
24. Griss P, von Andrian-Werburg H, Krempien B, et al. Biological-activity and histocompatibility of dense Al2O3- MgO ceramic implants in rats. J Biomed Mater Res. 1973;7(3):453-462.
25. Clarkin CE, Emery RJ, Pitsillides AA, Wheeler-Jones CP. Evaluation of VEGF-mediated signaling in primary human cells reveals a paracrine action for VEGF in osteoblast-mediated crosstalk to endothelial cells. J Cell Physiol. 2008;214(2):537-544.